HHS Public Access

Author manuscript

*J Neurosci Res*. Author manuscript; available in PMC 2022 March 29.

Published in final edited form as:

*J Neurosci Res*. 2022 February ; 100(2): 638–652. doi:10.1002/jnr.24982.

# Deletion of transcription factor AP-2β from the developing murine trabecular meshwork region leads to progressive glaucomatous changes

**Aftab Taiyab**[1], **Monica Akula**[1], **Japnit Dham**[1], **Paula Deschamps**[1], **Heather Sheardown**[2], **Trevor Williams**[3], **Teresa Borrás**[4], **Judith A. West-Mays**[1]

[1]Department of Pathology and Molecular Medicine, McMaster University, Hamilton, ON, Canada

[2]Department of Chemical Engineering, McMaster University, Hamilton, ON, Canada

[3]Department of Craniofacial Biology, University of Colorado, Aurora, CO, USA

[4]Department of Ophthalmology, University of North Carolina School of Medicine, Chapel Hill, NC, USA

## Abstract

Glaucoma is one of the leading causes of irreversible blindness and can result from abnormalities in anterior segment structures required for aqueous humor outflow, including the trabecular meshwork (TM) and Schlemm's canal (SC). Transcription factors such as AP-2β play critical roles in anterior segment development. Here, we show that the *Mgp*-Cre knock-in (*Mgp*-Cre.KI) mouse can be used to target the embryonic periocular mesenchyme giving rise to the TM and SC. Fate mapping of male and female mice indicates that AP-2β loss causes a decrease in iridocorneal angle cells derived from *Mgp*-Cre.KI-expressing populations compared to controls. Moreover, histological analyses revealed peripheral iridocorneal adhesions in AP-2β mutants that were accompanied by a decrease in expression of TM and SC markers, as observed using immunohistochemistry. In addition, rebound tonometry showed significantly higher intraocular

**Correspondence** Judith A. West-Mays, Department of Pathology and Molecular Medicine, McMaster University, 1200 Main Street West, L8N 3Z5, Hamilton, ON, Canada. westmayj@mcmaster.ca.
Aftab Taiyab and Monica Akula should be considered joint first authors.

AUTHOR CONTRIBUTIONS

All authors had full access to all the data in the study and take responsibility for the integrity of the data and the accuracy of the data analysis. *Conceptualization*, J.W.M., T.W., A.T., M.A., and J.D.; *Methodology*, J.W.M., T.W., A.T., M.A., and J.D.; *Investigation*, A.T., M.A., J.D., and P.D.; *Formal Analysis*, A.T., M.A., and J.D.; *Resources*, J.W.M., T.B., T.W., and H.S.; *Writing – Original Draft*, J.W.M., T.W., T.B., H.S., A.T., M.A., and J.D.; *Writing – Review & Editing*, J.W.M., T.W., T.B., H.S., A.T., M.A., and J.D.; *Visualization*, A.T., M.A., and J.D.; *Supervision*, J.W.M. and A.T.; *Project Administration*, J.W.M.; *Funding Acquisition*, J.W.M. and T.W.

CONFLICT OF INTEREST

The authors declare no conflict of interest.

DECLARATION OF TRANSPARENCY

The authors, reviewers and editors affirm that in accordance to the policies set by the *Journal of Neuroscience Research*, this manuscript presents an accurate and transparent account of the study being reported and that all critical details describing the methods and results are present.

PEER REVIEW

The peer review history for this article is available at https://publons.com/publon/10.1002/jnr.24982.

SUPPORTING INFORMATION

Additional supporting information may be found in the online version of the article at the publisher's website.

pressure (IOP) that was correlated with a progressive significant loss of retinal ganglion cells, reduced retinal thickness, and reduced retinal function, as measured using an electroretinogram, in AP-2β mutants compared with controls, reflecting pathology described in late-stage glaucoma patients. Importantly, elevated IOP in AP-2β mutants was significantly reduced by treatment with latanoprost, a prostaglandin analog that increases unconventional outflow. These findings demonstrate that AP-2β is critical for TM and SC development, and that these mutant mice can serve as a model for understanding and treating progressive human primary angle-closure glaucoma.

**Keywords**

glaucoma; outflow pathways; periocular mesenchyme; RRID:AB_143157; RRID:AB_2058198; RRID:AB_2077527; RRID:AB_2534074; RRID:AB_2534102; RRID:AB_2536161; RRID:AB_2749865; RRID:AB_476701; RRID:AB_626765

## 1 | INTRODUCTION

Glaucoma is one of the leading causes of irreversible blindness worldwide, with 111.8 million individuals projected to be affected by the end of 2040 (Quigley & Broman, 2006; Tham et al., 2014). There are two major types of glaucoma, which are primary open-angle glaucoma and primary angle-closure glaucoma, with increased intraocular pressure (IOP) being a risk factor for both types (Weinreb et al., 2014). IOP results from the balance between aqueous humor secretion from the ciliary body found posterior to the iris (Civan & Macknight, 2004) and aqueous humor outflow through the drainage structures in the iridocorneal angle that include the trabecular meshwork (TM) and Schlemm's canal (SC) (Civan & Macknight, 2004). The blockade of outflow can lead to elevated IOP (Lee et al., 2006), which can put mechanical stress on the optic nerve head (ONH), causing progressive degeneration of retinal ganglion cells (RGCs) (Gould & John, 2002) and eventual vision loss. The obstruction of aqueous humor outflow can arise from adhesions between the iris and cornea, such as a peripheral iridial adhesion to the cornea, also known as peripheral anterior synechia (PAS) (Lee et al., 2006).

Primary angle-closure glaucoma can result from anterior segment dysgenesis (ASD), in which structures found in the anterior segment of the eye, including the lens, ciliary body, iris, cornea, TM, and SC, develop abnormally (Gould & John, 2002; Wright et al., 2016). The embryonic tissue types that contribute to these structures include the surface ectoderm and the periocular mesenchyme (POM) consisting of cranial neural crest cells (NCCs) and paraxial mesoderm cells (Gage et al., 2005; Gould et al., 2004). Of particular importance for glaucoma are the TM and SC, since they regulate aqueous outflow (Gould et al., 2004). In mice at embryonic day (E) 15.5, POM cells migrate into the region between the anterior rim of the optic cup and the developing corneal endothelium, with this population of cells giving rise to the stroma of the iris and ciliary body, as well as the TM and SC (Cvekl & Tamm, 2004). Between postnatal day (P) 1 and P4, POM cells can be found at the iridocorneal angle between the newly forming iris and cornea (Cvekl & Tamm, 2004; Smith et al., 2001). Between P4 and P10, POM cells elongate, flatten, and begin differentiating into TM cells

that secrete extracellular matrix components, while blood vessels form in the scleral region (Cvekl & Tamm, 2004; Smith et al., 2001). By P14, extracellular matrix fibers secreted by the developing TM cells form beams, with these cells wrapping around the beams and the blood vessels at the iridocorneal angle adjacent to the sclera fusing to form SC, both of which play a vital role in aqueous humor outflow (Cvekl & Tamm, 2004; Kizhatil et al., 2014).

A number of genes have been shown to regulate development of the anterior segment in mice (Chen & Gage, 2016; Cross et al., 2014; Liu & Johnson, 2010; Romero et al., 2011; Smith et al., 2000; Tümer & Bach-Holm, 2009), including the activating protein 2 (AP-2) transcription factor family members, such as AP-2α and AP-2β (Barzago et al., 2017; Bassett et al., 2007, 2010, 2012; Chen et al., 2016; Kerr et al., 2014; Pontoriero et al., 2008; West-Mays et al., 1999). Specifically, AP-2β, encoded by the *Tfap2b* gene, is expressed in mouse POM cells that migrate into the region between the anterior rim of the optic cup and cornea and that also give rise to the TM and SC (Bassett et al., 2012; Martino et al., 2016). AP-2β null mice show eye defects; however, since these mice do not survive postnatally, they do not allow for assessment of pathology that arises at later stages (Moser et al., 1997). Therefore, we previously used the Wnt1Cre transgenic line to conditionally delete AP-2β from cranial NCCs (AP-2β NCC KOs), allowing such mutant mice to be followed into adulthood (Martino et al., 2016). The resulting mice showed anterior segment defects, including loss of the corneal endothelium, a peripheral to central iridocorneal adhesion, and absence of formation of a TM region (TMR) and SC, in addition to increased IOP and glaucomatous features (Akula et al., 2020; Martino et al., 2016). However, it was unclear whether the peripheral to central iridocorneal adhesion, or the lack of a TM and SC due to AP-2β deletion contributed to the increased IOP and glaucomatous features. This study sets out to distinguish between a cell-autonomous versus a non-cell autonomous role for AP-2β in TM cell development by using a more specific Cre mouse line to delete AP-2β from the TMR. The matrix GLA protein (Mgp) Cre mouse line expresses Cre in the iridocorneal angle region in the adult mouse, in addition to the peripapillary scleral region and retinal vascular bed (Asokan et al., 2018; Borrás et al., 2015). Due to this specific localization of Cre expression to the iridocorneal angle region, the *Mgp*-Cre knock-in (*Mgp*-Cre.KI) mouse line was used to study the effect of AP-2β deletion from the TMR. Mutant mice, termed the AP-2β TMR knockouts (AP-2β TMR KOs), underwent normal POM cell migration, but displayed the absence of a morphologically distinct TMR, in addition to partial angle closure and a reduction in expression of the TM markers, αSMA and myocilin, and SC markers, Prox1 and endomucin. These mice further developed increased IOP at 1 month of age, accompanied by a significant reduction in the number of RGCs and reduced retinal function, making this a model of human primary angle-closure glaucoma.

## 2 | MATERIALS AND METHODS

### 2.1 | Animal husbandry

All procedures were conducted in accordance with the Association for Research in Vision and Ophthalmology Statement for the Use of Animals in Ophthalmic and Vision Research, and were approved by McMaster University's Animal Research Ethics Board. In the AP-2β

TMR KO and AP-2β NCC KO mouse models used in the current study, the *Tfap2b* gene was deleted using either a Cre transgene under control of the *Mgp* gene (Borrás et al., 2015) or the *Wnt1* gene (*H2az2*$^{Tg(Wnt1\text{-}cre)11Rth}$ Tg(Wnt1-GAL4)11Rth/J, Jackson Lab, Bar Harbor, ME). Either male *Mgp*-Cre.KI$^{+/-}$; *Tfap2b*$^{+/-}$ mice or male *Wnt1Cre*$^{+/-}$; *Tfap2b*$^{+/-}$ mice were bred with female *Tfap2b*$^{lox/lox}$ to generate *Mgp*-Cre.KI$^{+/-}$; *Tfap2b*$^{-/lox}$ mice (AP-2β TMR KOs) and *Wnt1Cre*$^{+/-}$; *Tfap2b*$^{-/lox}$ mice (AP-2β NCC KOs), respectively, as well as age-matched control littermates. In addition, male *Mgp*-Cre.KI$^{+/-}$; *Tfap2b*$^{+/-}$ mice were bred with *Tfap2b*$^{lox/lox}$; *tdTomato*$^{lox/lox}$ mice (the tdTomato reporter was the B6; 129S6-Gt (ROSA)26Sortm14(CAG-tdTomato)Hze/J strain from the Jackson Lab) to generate *Mgp*-Cre. KI$^{+/-}$; *Tfap2b*$^{-/lox}$; *tdTomato*$^{lox/+}$ mice in order to assess *Mgp*-Cre.KI expression. All genotyping was carried out using standard PCR protocols (Martino et al., 2016). Inbreeding between mouse lines used for the final cross was avoided, an equal number of both male and female mice obtained from the final cross were used for experiments, and C57BL/6J was the background strain used for all genetic crosses (Charles River, Wilmington, MA). All animals were housed in groups of up to five animals within enriched cages cleaned weekly and kept under a 12-hr light and 12-hr dark cycle at 25°C.

## 2.2 | Histology

The eyes were enucleated from euthanized mice, and fixed in 4% paraformaldehyde (PFA) for 24 hr at 4°C, followed by storage in 70% ethanol for paraffin sections, or in 30% sucrose overnight at 4°C for frozen sections. The eyes were then processed and embedded in paraffin wax or optimal cutting temperature compound. Paraffin tissue blocks were sectioned at a thickness of 4 μm and subsequently stained using hematoxylin and eosin (H&E), or immunohistochemistry (IHC) was carried out. Frozen tissue blocks were sectioned at a thickness of 10 μm to assess tdTomato expression (Bassett et al., 2007).

## 2.3 | Immunohistochemistry

IHC was performed as previously described (Akula et al., 2020). Primary antibodies included AP-2β (1:50, Cell Signaling, 2509S, Danvers, MA), α-smooth muscle actin (αSMA, 1:100, Sigma Aldrich, A2547, Oakville, ON), myocilin (1:200, FabGennix, MYO-101AP, Frisco, TX), endomucin (1:100, eBioscience, 14–5851-82, San Diego, CA), Prox1 (1:100, Covance, 925201, Princeton, NJ), N-cadherin (1:100, BD Transduction, 610920, San Jose, CA), and Brn3a (1:100, sc-8429, Santa Cruz, CA) (Bassett et al., 2012; Martino et al., 2016; Robertson et al., 2013; Taiyab et al., 2021) (Table 1). Alexa Fluor secondary antibodies (1:200, Invitrogen, Molecular Probes, Burlington, ON) were used to detect the primary antibodies, and slides were mounted with ProLong Gold containing DAPI (4′,6-diamidino-2-phenylindole) (Thermofisher, Waltham, MA). To analyze tdTomato expression for the fate mapping experiments, frozen sections of the eyes from control and AP-2β TMR KO mice crossed with the tdTomato mouse line were used. All sections were imaged using a Leica DM6 B microscope with a bright-field or fluorescence attachment, and images were acquired using a high-resolution camera and LasX imaging software.

## 2.4 | Immunohistochemistry of flat mounted retinas

The eyes were fixed in 4% PFA for 2 hr at room temperature and washed three times for 10 min per wash in PBS, after which retinas were dissected out and permeabilized overnight

at room temperature in a solution of 0.3% Triton X mixed in PBS (PBST) (Hicks et al., 2018). Retinas were blocked in normal serum with PBST for 3 hr at room temperature, and agitated in a 1:100 dilution of Brn3a antibody (Santa Cruz, CA) mixed with 1% DMSO and 5% normal serum in PBST for 72 hr at 4°C. Retinas were then washed in PBST and agitated in secondary antibody at a 1:200 dilution along with 1% DMSO and 2.5% normal serum in PBST for 4 hr at room temperature, after which retinas were washed in PBS, flat mounted using mounting medium containing DAPI and coverslipped.

### 2.5 | Optical coherence tomography (OCT)

For all *in vivo* experiments, mice were deeply anesthetized with 2.5% avertin, and eye drops (Alcon, Mississauga, CA) were applied to prevent the cornea from drying. For live imaging of the eye, the cornea was positioned 1–2 cm from the Phoenix Micron IV anterior segment imaging system with an OCT attachment (Phoenix Research Labs, Pleasanton, CA).

### 2.6 | Intraocular pressure measurement

Eye drops (Alcon, Mississauga, CA) were applied to the corneas of anesthetized mice to prevent them from drying, and a minimum of six IOP values were acquired from each eye using a rebound tonometer (TonoLab, Vantaa, Finland), with each value being an average of six measurements (Martino et al., 2016).

### 2.7 | Latanoprost treatment

In order to test whether the unconventional pathway may be functional in the AP-2β TMR KO, the eyes of anesthetized control, TMR KO, and NCC KO mice were all treated topically with 0.005% latanoprost (Pfizer, New York, NY), a prostaglandin analog. Prostaglandins are a class of compounds that increase unconventional outflow by relaxing the ciliary muscle and by reducing the amount of extracellular matrix between the ciliary muscle fibers, both of which serve to increase the space between the fibers (Winkler & Fautsch, 2014). IOP was acquired immediately before treatment, as well as 20 min, 1 hr, and 24 hr post-treatment.

### 2.8 | Electroretinograms (ERGs)

P45 and 2- to 3-month-old control and AP-2β TMR KO mice were used to perform scotopic full-field ERGs (Phoenix Research Laboratories, Pleasanton, CA). Animals were anesthetized as described, their pupils dilated with 0.5% tropicamide (AKORN, Lake Forest, IL) and eye drops applied to prevent the cornea from drying. A ground electrode was placed in the tail, while a reference electrode was placed in the scalp, and the eye was positioned such that the cornea made contact with the corneal electrode (Hicks et al., 2018). The retinal responses to 2-ms flashes of LED light (504 nm) at light intensities between −0.2 and 2.5 $cd{\cdot}s/m^2$ (on a log scale) were recorded, and 20 responses were measured for the lowest intensity, while five were measured for the highest intensity.

### 2.9 | Statistics

An equal number of control and mutant mice, as well as an equal number of male and female mice of the required ages were randomly assigned to each experiment, and a minimum of three eyes were used for each experiment to allow for statistical analysis. Each

experiment was replicated a minimum of three times, and no data or outliers were removed from the analysis. Cell counts of Brn3a-positive cells in control and AP-2β TMR KO mice were carried out using the manual cell counter plugin on ImageJ. Furthermore, thickness of the total retina, the outer nuclear layer (ONL), the INL, and the IPL were measured using the line tool on ImageJ. The sections used for the statistical analyses were matched by the level of the section, including by the diameter of the ocular lens, and three sections were evaluated per eye for all analyses. For analysis of retinal thickness and Brn3a cell counts in sections, three measurements were acquired per section, including one measurement at each peripheral region and one in the central retina, which were averaged for each section. For flat mounted retinas, Brn3a-positive cells were counted in three separate regions, which included the region adjacent to the ONH, the mid-periphery, and the peripheral retina, and these measurements were acquired in four different retinal petals (Figure S4).

In order to compare the difference in the mean values for IOP, cell counts in flat mounted retinas and retinal sections, as well as thickness of retinal layers between control and AP-2β TMR KO animals, which were two independent groups, a two-sided independent *t* test was performed on GraphPad Prism 9.0. For ERG studies, all a- and b-wave amplitude values acquired for each presented intensity were included in the analysis. As part of this analysis, there were two independent variables, which were the genotype of the mouse and the flash intensity, and the measurements were acquired in the same set of mice by increasing the flash intensity values after acquiring the a-wave and b-wave amplitudes in response to each intensity. Consequently, differences in the mean values of the a-wave and b-wave amplitudes between control and TMR KO mice in response to increasing flash intensities were analyzed using either a two-way repeated measures ANOVA or a mixed model. If significance was found, multiple comparisons were performed using the Bonferroni method. IOP in controls and both types of mutants were analyzed before latanoprost treatment and at various time points after treatment using a two-way repeated measures ANOVA. This test was used because there were two independent variables, which were genotype and time after latanoprost treatment, and IOP was measured in the same set of mice over time. If significance was found, Tukey's post hoc test was carried out. For all statistical analyses, a *p*-value of less than 0.05 was considered statistically significant.

## 3 | RESULTS

### 3.1 | Fate mapping of iridiocorneal angle tissue using the Mgp-Cre.KI reveals a loss of derivative cell populations in AP-2β TMR KOs

The *Mgp*-Cre.KI mouse line has previously been characterized for its function in the adult eye, where it has been shown to target cells in the iridocorneal angle region, as well as the peripapillary scleral region and retinal vascular bed (Asokan et al., 2018; Borrás et al., 2015). Mgp is also expressed in embryonic mouse tissues (Luo et al., 1995), and we therefore reasoned that *Mgp*-Cre.KI might be active during the perinatal period of mouse eye development. To test this hypothesis, male *Mgp*-Cre.KI mice were crossed with tdTomato females, and the expression of the Cre-activated tdTomato reporter was tracked beginning at E15.5 when the POM that gives rise to the TM during ocular development is being populated by the neural crest (Cvekl & Tamm, 2004). At E15.5, mice heterozygous

for the *Mgp*-Cre.KI transgene expressed tdTomato in the developing POM region at the anterior rim of the optic cup (Figure 1a). At P1 (Figure 1c), tdTomato expression was present in the iridocorneal angle region of control mice, and there was a similar pattern of expression at P4, P7, and P14 (Figure 1e,g,i). Notably, though, neither the corneal endothelium nor stroma, additional derivatives of the NCC-derived POM, are strongly marked by *Mgp*-Cre.KI in contrast to the results obtained using the Wnt1Cre transgene which also targets these tissues (Akula et al., 2020; Martino et al., 2016).

Next, the *Mgp*-Cre.KI mouse line was used to delete AP-2β from the iridocorneal angle region and examine the effect of AP-2β deletion on TM development. In this instance, fate mapping showed that there was no overt difference in tdTomato cell populations between the AP-2β TMR KO compared with control mice at either E15.5 or P1 (Figure 1a–d; $n$ = 3 eyes). However, by P4 ($n$ = 3 eyes), P7 ($n$ = 3 eyes), and P14 ($n$ = 3 eyes), there was a reduction in tdTomato expression in the iridocorneal angle region of TMR KO mice (Figure 1f,h,j, asterisks), when compared with the developing angle of control mice (Figure 1e,g,i). These findings indicate that AP-2β is required for appropriate development and/or maintenance of these iridiocorneal angle populations.

### 3.2 | AP-2β TMR KOs display partial angle closure, and reduced expression of TM and SC markers

The overall morphology of the AP-2β TMR KO eyes at P14, as shown by H&E stained sections, revealed partial iridocorneal angle closure due to PAS of the iris to the cornea (Figure 2a,b; $n$ = 6 eyes). There was also a small amount of variability in the degree of angle closure within the same eye (Figure 2). In order to confirm histological observations of the partially closed iridocorneal angle in TMR KOs, *in vivo* imaging was carried out using OCT. At P45 (Figure 2g,h), control mice showed a completely open iridocorneal angle, while AP-2β TMR KO mice displayed a partially open iridocorneal angle resembling PAS. Since the absence of a corneal endothelium is known to contribute to adherence of the iris to the cornea (Reneker et al., 2000; Waring et al., 1982), IHC for N-cadherin was performed, and this experiment demonstrated that the corneal endothelium was present in the TMR KO mice, although its appearance was more discontinuous than in controls (Figure 2i,j; $n$ = 3 eyes). Additionally, at P14, a distinct TM region was not visible in the AP-2β TMR KO eyes (Figure 2d,f, arrowhead) when compared to control eyes (Figure 2c,e). To assess the deletion of AP-2β in the TM, IHC was performed using antibodies specific for AP-2β and αSMA, a marker of the TM. AP-2β was observed to be completely absent in the TM region of P14 AP-2β TMR KO mice when compared to control mice (Figure 3a, TMR KO panel, brackets, inset), although there was no difference in expression in the retina (Figure S2). Furthermore, a marked reduction in αSMA expression was observed in the TMR KO when compared with control mice (Figure 3a, panel marked “control”; brackets; $n$ = 6 eyes). There was also a prominent reduction in expression of myocilin, another TM marker, in the iridocorneal angle of TMR KO eyes (Figure 3b; $n$ = 6 eyes) compared with control eyes. In addition to the TM, SC is also part of the conventional outflow pathway that is blocked in primary angle-closure glaucoma. Consequently, IHC was carried out for markers of SC, and TMR KOs showed reduced expression of SC markers, Prox1 (Figure 3c; arrowheads) and endomucin (Figure 3c; arrows), when compared with controls.

### 3.3 | AP-2β TMR KOs have increased IOP that reduces with latanoprost treatment

To determine whether abnormalities in the TM and SC are leading to an increase in IOP, measurements were acquired from both TMR KO and control mice at P30. There was a significant increase in IOP in TMR KOs when compared with controls at P30 ($n = 10$ eyes; two-sided independent $t$ test; $t_{18} = 12.57$; $p < 0.0001$) (Figure 4a). Since the TMR KOs possessed a partially open iridocorneal angle, the functionality of the unconventional outflow pathway was tested by treating 2- to 3-month-old AP-2β TMR KOs with latanoprost, a prostaglandin analogue that increases outflow through the unconventional pathway (Aihara et al., 2002). For comparison, the same assay was performed either in control mice or AP-2β NCC KO mice, the latter having a complete peripheral to central iridial adhesion to the cornea (Martino et al., 2016). Twenty minutes after latanoprost treatment of the AP-2β TMR KO, there was a significant reduction in IOP ($n = 6$ eyes; two-way repeated measures ANOVA, Tukey's post hoc test; $F_{(2,40)} = 169.8$) when compared to its baseline value (Figure 4b). By 60 min of post-treatment, IOP in the TMR KO increased back to its baseline level ($p < 0.0001$), and this continued to be the case at 24-hr post-treatment ($p < 0.0001$). On the other hand, the AP-2β NCC KO mice retained a high IOP compared to controls even after latanoprost treatment ($n = 6$ eyes; $p < 0.0001$ at all time points), demonstrating that the completely closed angle phenotype has prevented functionality of both the conventional and unconventional pathways. These findings indicate that the two AP-2β mutant models have different effects on disrupting the conventional and unconventional outflow pathways in that IOP in the TMR KO can be reduced by latanoprost acting through the latter pathway, whereas this treatment has no benefit in the NCC KO model.

### 3.4 | Increased IOP is correlated with additional glaucomatous changes in AP-2β TMR KOs

To determine whether the increased IOP observed in the AP-2β TMR KO mice is correlated with additional glaucomatous changes, H&E staining of the retina was performed. This analysis revealed a significant reduction in thickness of the total retina, the inner nuclear layer (INL), and inner plexiform layer (IPL) at both P30 (a minimum of $n = 3$ eyes; two-sided independent $t$ test for thickness of the total retina and each separate layer; total retina, $t_6 = 4.12$, $p < 0.01$; INL, $t_6 = 4.83$, $p < 0.01$; IPL, $t_6 = 3.68$, $p < 0.05$) and P40 (a minimum of $n = 3$ eyes; total retina, $t_5 = 3.05$, $p < 0.05$; INL, $t_5 = 3.04$, $p < 0.05$; IPL, $t_5 = 4.11$, $p < 0.01$) (Figure 5a,b) as compared to controls. Furthermore, while at P14 there was no difference in expression of Brn3a, a marker of RGCs, by P30 and P40, reduced expression was found in TMR KO sections when compared with controls (Figure S3). IHC studies using flat mounted retinas from the P60 control and TMR KO showed that there was a significant reduction in the number of Brn3a-positive cells in the region adjacent to the ONH, the mid-periphery, and peripheral retina (analyzed regions marked in Figure S4) in TMR KOs when compared to controls (Figure 5c,d; $n = 6$ eyes; two-sided independent $t$ test for all three regions; $t_{10} = 25.87$ for the ONH, $t_{10} = 24.69$ for the mid-peripheral region, $t_{10} = 20.19$ for the peripheral region; $p < 0.0001$ for all three regions). In addition, as seen using a full-field scotopic flash ERG, although at P45 there was no difference in a-wave and b-wave amplitudes between TMR KOs and controls (Figure 6; $F_{(1,6)} = 0.15$ for the a-wave; $F_{(1,6)} = 0.79$ for the b-wave; two-way repeated measures ANOVA), a significant reduction

in the a-wave and b-wave amplitudes of 2- to 3-month-old TMR KO animals was observed when compared with age-matched control animals (Figure 7a–c; a minimum of $n = 3$ mice; mixed model, Bonferroni post hoc method; $F_{(1,10)} = 12.81$ for the a-wave; $F_{(1,10)} = 37.00$ for the b-wave; $p < 0.05$ for the last three flash intensities tested for both the a-wave and b-wave amplitudes).

## 4 | DISCUSSION

Glaucoma is one of the major causes of irreversible blindness worldwide. Thus, understanding the mechanisms underlying this disease is important and necessary in order to develop treatments. Primary angle-closure glaucoma is typically a disorder involving dysgenesis of anterior segment structures required for regulating IOP either through the conventional pathway, including the TM and SC, or the unconventional pathway that includes the ciliary muscle (Gould & John, 2002; Gould et al., 2004). Therefore, it is imperative to understand the role of genes that regulate the development of anterior angle structures. The AP-2β TMR KO mice with AP-2β deleted from the developing iridocorneal angle region not only showed abnormal development of the TM and SC, but also exhibited increased IOP and progressive glaucomatous features, including reduced retinal thickness, RGC cell loss, and reduced retinal function.

Previously, our laboratory had created the AP-2β NCC KO mouse model in which the Wnt1Cre mouse line was used to delete AP-2β from the cranial neural crest (Akula et al., 2020). These mice showed defects in the TM required for aqueous outflow, which hinted at a cell-autonomous role for AP-2β in TM development. However, the Wnt1Cre system used to knock out AP-2β was broadly and strongly expressed in multiple neural crest derivatives, including not only the TM but also the corneal stroma and endothelium (Akula et al., 2020; Martino et al., 2016). Consequently, it is possible that the corneal defects leading to the peripheral to central iridocorneal adhesion may have resulted in secondary defects in the TM in AP-2β NCC KO mice (Cvekl & Tamm, 2004). This study aimed to further delineate the role of AP-2β specifically in development of the TM by using a Cre transgenic line, *Mgp*-Cre.KI, that was previously shown to target cells in the iridocorneal angle region by adult stages (Borrás et al., 2015) to conditionally delete AP-2β from the developing TMR. *Mgp*-Cre.KI expression was observed in the developing POM giving rise to the TM and SC, but expression in corneal cell types was much more reduced when compared to the Wnt1Cre, suggesting that the *Mgp*-Cre.KI can be used to more specifically target TM development. This is the first study to show the developmental expression pattern of *Mgp*-Cre.KI, particularly at early postnatal time points relevant for TM development and expands the genetic tools available for the analysis of gene function during development of the anterior segment.

Fate mapping in the AP-2β TMR KO mice using the tdTomato mouse line showed no difference between controls and TMR KOs in the migration of the POM cells contributing to TM tissue prenatally (Figure 1a,b). However, reduced expression of tdTomato in the iridocorneal angle region of TMR KO mice was observed at early postnatal stages (Figure 1e–j) when compared to control mice. The combined observations from fate mapping at postnatal stages and the reduction in expression of TM markers (Figure 3a,b) support the

idea that AP-2β is directly involved in TM development. On the other hand, the reduced expression of SC markers could be attributed to the PAS phenotype observed in the AP-2β TMR KO. It has been shown that the development of SC relies on TM-mediated pressure-induced expression of transcription factors, such as Klf4 (Choi et al., 2017). Moreover, the TM/conventional outflow pathway was observed to be absent in the TMR KO mutants, which might be contributing to the hypoplastic appearance of SC, as demonstrated by endomucin staining (Figure 3c). Although the TMR KO model targets TM development more specifically than the NCC KO model, it is possible that PAS in the TMR KO could indirectly be leading to abnormal TM development at the iridocorneal angle. Consequently, one way to further target the specific role of AP-2β would be to use temporal Cre mice in which *Tfap2b* is deleted after corneal development is complete and during the developmental window when TM cells begin to develop and differentiate.

The iridocorneal angle defects in AP-2β TMR KO mice were accompanied by a significantly increased IOP as compared to littermates, and this is likely due to the fact that the conventional outflow pathway is blocked because of the absence of a TM and hypoplasticity of SC. However, the unconventional outflow pathway appeared to be functional in these mutants, since the IOP of the TMR KO was reduced 20 min after treatment with latanoprost when contrasted with its baseline IOP value. In comparison, in the AP-2β NCC KO mice used as a negative control, the peripheral to central iridocorneal adhesion prevents outflow through both the conventional and unconventional pathways. As a result, the NCC KO did not exhibit a decrease in IOP following latanoprost treatment. In addition, although the unconventional pathway is functional in the TMR KO, this model displayed similar IOP levels as the NCC KO model (Martino et al., 2016), possibly because unconventional outflow is largely pressure insensitive (Johnson et al., 2017). The lack of a sustained effect of latanoprost in mice when compared with humans (Alm, 2014; Garcia-Sanchez et al., 2004; Parrish et al., 2003; Toris et al., 1999) could be because of the greater percentage of unconventional outflow in mice compared with humans (Johnson et al., 2017). Since conventional outflow is dysfunctional in mouse and human eyes with glaucoma, and since the unconventional pathway accounts for a greater percentage of outflow in mice, latanoprost may be getting cleared from the TMR KO mouse anterior chamber at a more rapid rate compared with the glaucomatous human anterior chamber. Moreover, aqueous humor turnover would further dilute the working concentration of the latanoprost (0.005%, Xalatan), which partially explains the rapid return of the IOP to the baseline value in TMR KO mice.

The TM and SC defects observed in the TMR KO likely resulted in the increased IOP. The significant reduction in the thickness of the retina, the INL, and IPL, as well as the reduction in the number of Brn3a-positive cells in P60 flat mounted retinas in the TMR KOs when compared with control mice suggest that the elevated IOP is leading to glaucomatous defects in the retina. High IOP in mice has previously been reported to induce thinning of the IPL (Martino et al., 2016), and our current results are in agreement with these observations. Previous studies using mouse models in which increased IOP was induced using microbead injections also reported thinning of the INL combined with a reduction in the expression of markers of specific amacrine cell subtypes (Akopian et al., 2019; Gunn et al., 2011), which

is one possible explanation for the reduction in the thickness of the INL observed in the TMR KO mice.

In addition to the reduction in the number of RGCs, a reduction in retinal function was also observed in the TMR KOs using a full-field scotopic flash ERG. It was previously not possible to carry out ERGs in the AP-2β NCC KO mice, since the central cornea adhered to the lens and caused corneal cataracts (Martino et al., 2016). However, in the TMR KO, the adhesion was absent and the corneas were more transparent, enabling evaluation of retinal function using an ERG. Particularly, there was a reduction in the amplitude of both the a-wave and b-wave that occurred after P45. The a-wave represents the response of photoreceptors to a flash of light in this particular type of ERG, whereas the b-wave represents the depolarization response of inner retinal cells downstream of the photoreceptors, including the bipolar cells and Müller glia, but potentially also the RGCs and amacrine cells (Dong & Hare, 2000; Miura et al., 2009; Smith et al., 2014). The observed decline in b-wave amplitude possibly represents a reduction in RGC function caused by the loss of RGCs as assessed by Brn3a staining. Furthermore, since the INL is significantly thinner in TMR KOs, changes in this layer, which includes amacrine and bipolar cells, may also be contributing to the b-wave phenotype. We hypothesize that the reduction in a-wave amplitude results from reduced photoreceptor numbers or a reduction in photoreceptor outer segment length, since the latter is commonly observed in the DBA/2J glaucoma mouse model (Bayer et al., 2001; Harazny et al., 2009). Future studies will be needed to distinguish between these various possibilities.

A number of mouse models of glaucoma, including mechanically induced models, such as the optic nerve crush model and models that develop spontaneous mutations resulting in glaucomatous features, such as the DBA/2J model, have been developed to understand the progression of glaucoma (Johnson & Tomarev, 2010). In addition, targeted gene deletion models including mice with mutations in *Sh3pxd2b* (Mao et al., 2011), *Pitx2* (Chen & Gage, 2016), *Foxc1*, *Foxc2* (Smith et al., 2000), and *Lmx1b* (Liu & Johnson, 2010), as well as the AP-2β NCC KO mouse established previously in our laboratory (Martino et al., 2016), all of which have ASD, show the role of these genes in the etiology and pathophysiology of glaucoma. Although the DBA/2J model is an effective model of glaucoma, it requires time to develop high IOP and does not always result in a consistent phenotype. Furthermore, the microbead model requires careful experimental manipulation for the best and consistent results (Johnson & Tomarev, 2010). On the other hand, the AP-2β TMR KO is an acute model of glaucoma that consistently shows increased IOP.

*Tfap2b* has been associated with a human disorder, Char syndrome, and while ocular abnormalities have not been reported in this condition, the rarity and severity of this condition could explain the lack of documented ocular defects (Satoda et al., 2000). Moreover, the human *PITX2* gene has been associated with ASD in humans (Tumer & Bach-Holm, 2009), and since in mice, *Tfap2b* has been shown to be a downstream effector of the *Pitx2* gene (Chen et al., 2016), this suggests that the human *TFAP2B* gene may also be associated with human ASD. Here, we demonstrate that specific deletion of *Tfap2b* from the developing iridocorneal angle using the *Mgp*-Cre.KI (Borrás et al., 2015) leads to partial angle closure and defects in the TM and SC, and the resulting increase in IOP

in the TMR KO combined with the progressive loss of RGCs, thinning of the retina and a reduction in retinal function makes this a useful animal model of human primary angle-closure glaucoma. As a potential model of primary angle-closure glaucoma, we also propose that the AP-2β TMR KO mouse can be employed to investigate the effects and physiological mechanisms of IOP-lowering drugs, as well as to study and demonstrate the effect of new and existing neuroprotective strategies.

## Supplementary Material

Refer to Web version on PubMed Central for supplementary material.

## ACKNOWLEDGMENTS

This work was supported by the National Institutes of Health (grant number R01 EY025789) (JWM, TW), USA. AT acknowledges Ontario Research Funding (ORF - ORF RE 08 042), Canada for financial support. MA acknowledges the Ontario Graduate Scholarship (OGS), Canada for funding.

## DATA AVAILABILITY STATEMENT

All data used in this study have been included in the supplementary table file.

## REFERENCES

Aihara M, Lindsey JD, & Weinreb RN (2002). Reduction of intraocular pressure in mouse eyes treated with latanoprost. Investigative Ophthalmology & Visual Science, 43(1), 146–150. [PubMed: 11773025]

Akopian A, Kumar S, Ramakrishnan H, Viswanathan S, & Bloomfield SA (2019). Amacrine cells coupled to ganglion cells via gap junctions are highly vulnerable in glaucomatous mouse retinas. Journal of Comparative Neurology, 527(1), 159–173. 10.1002/cne.24074

Akula M, Taiyab A, Deschamps P, Yee S, Ball AK, Williams T, & West-Mays JA (2020). AP-2beta is required for formation of the murine trabecular meshwork and Schlemm's canal. Experimental Eye Research, 195, 108042. 10.1016/j.exer.2020.108042 [PubMed: 32353428]

Alm A (2014). Latanoprost in the treatment of glaucoma. Clinical Ophthalmology, 8, 1967–1985. 10.2147/OPTH.S59162 [PubMed: 25328381]

Asokan P, Mitra RN, Periasamy R, Han Z, & Borras T (2018). A naturally fluorescent Mgp transgenic mouse for angiogenesis and glaucoma longitudinal studies. Investigative Ophthalmology & Visual Science, 59(2), 746–756. 10.1167/iovs.17-22992 [PubMed: 29392320]

Barzago MM, Kurosaki M, Fratelli M, Bolis M, Giudice C, Nordio L, Cerri E, Domenici L, Terao M, & Garattini E (2017). Generation of a new mouse model of glaucoma characterized by reduced expression of the AP-2β and AP-2δ proteins. Scientific Reports, 7, 11140. 10.1038/s41598-017-11752-6 [PubMed: 28894266]

Bassett E, Korol A, Deschamps P, Buettner R, Wallace V, Williams T, & West-Mays J (2012). Overlapping expression patterns and redundant roles for AP-2 transcription factors in the developing mammalian retina. Developmental Dynamics, 241(4), 814–829. 10.1002/dvdy.23762 [PubMed: 22411557]

Bassett E, Pontoriero G, Feng W, Marquardt T, Fini M, Williams T, & West-Mays J (2007). Conditional deletion of activating protein 2alpha (AP-2alpha) in the developing retina demonstrates non-cell-autonomous roles for AP-2alpha in optic cup development. Molecular and Cellular Biology, 27(21), 7497–7510. [PubMed: 17724084]

Bassett E, Williams T, Zacharias A, Gage P, Fuhrmann S, & West-Mays J (2010). AP-2alpha knockout mice exhibit optic cup patterning defects and failure of optic stalk morphogenesis. Human Molecular Genetics, 19(9), 1791–1804. [PubMed: 20150232]

Bayer AU, Neuhardt T, May AC, Martus P, Maag KP, Brodie S, Lütjen-Drecoll E, Podos SM, & Mittag T (2001). Retinal morphology and ERG response in the DBA/2NNia mouse model of angle-closure glaucoma. Investigative Ophthalmology & Visual Science, 42(6), 1258–1265. [PubMed: 11328737]

Borrás T, Smith M, & Buie L (2015). A novel Mgp-Cre knock-in mouse reveals an anticalcification/antistiffness candidate gene in the trabecular meshwork and peripapillary scleral region. Investigative Opthalmology & Visual Science, 56(4), 2203–2214.

Chen L, & Gage PJ (2016). Heterozygous Pitx2 null mice accurately recapitulate the ocular features of axenfeld-rieger syndrome and congenital glaucoma. Investigative Opthalmology & Visual Science, 57, 5023–5030.

Chen L, Martino M, Dombkowski A, Williams T, West-Mays J, & Gage PJ (2016). AP-2β is a downstream effector of PITX2 required to specify endothelium and establish angiogenic privilege during corneal development. Investigative Ophthalmology & Visual Science, 57(3), 1072–1081. 10.1167/iovs.15-18103 [PubMed: 26968737]

Choi D, Park E, Jung E, Seong YJ, Hong M, Lee S, Burford J, Gyarmati G, Peti-Peterdi J, Srikanth S, Gwack Y, Koh CJ, Boriushkin E, Hamik A, Wong AK, & Hong YK (2017). ORAI1 activates proliferation of lymphatic endothelial cells in response to laminar flow through Kruppel-like factors 2 and 4. Circulation Research, 120(9), 1426–1439. 10.1161/CIRCRESAHA.116.309548 [PubMed: 28167653]

Civan M, & Macknight A (2004). The ins and outs of aqueous humour secretion. Experimental Eye Research, 78(3), 625–631. [PubMed: 15106942]

Cross S, Macalinao D, McKie L, Rose L, Kearney A, Rainger J, Thaung C, Keighren M, Jadeja S, West K, Kneeland SC, Smith RS, Howell GR, Young F, Robertson M, van Thof R, John SWM, & Jackson IJ (2014). A dominant-negative mutation of mouse Lmx1b causes glaucoma and is semi-lethal via LDB1-mediated dimerization. PLoS Genetics, 10(5), e1004359. [PubMed: 24809698]

Cvekl A, & Tamm E (2004). Anterior eye development and ocular mesenchyme: New insights from mouse models and human diseases. BioEssays, 26(4), 374–386. 10.1002/bies.20009 [PubMed: 15057935]

Dong CJ, & Hare WA (2000). Contribution to the kinetics and amplitude of the electroretinogram b-wave by third-order retinal neurons in the rabbit retina. Vision Research, 40(6), 579–589. 10.1016/s0042-6989(99)00203-5 [PubMed: 10824262]

Gage P, Rhoades W, Prucka S, & Hjalt T (2005). Fate maps of neural crest and mesoderm in the mammalian eye. Investigative Ophthalmology & Visual Science, 46(11), 4200–4208. 10.1167/iovs.05-0691 [PubMed: 16249499]

Garcia-Sanchez J, Rouland JF, Spiegel D, Pajic B, Cunliffe I, Traverso C, & Landry J (2004). A comparison of the fixed combination of latanoprost and timolol with the unfixed combination of brimonidine and timolol in patients with elevated intraocular pressure. A six month, evaluator masked, multicentre study in Europe. British Journal of Ophthalmology, 88(7), 877–883. 10.1136/bjo.2003.029330

Gould DB, & John SW (2002). Anterior segment dysgenesis and the developmental glaucomas are complex traits. Human Molecular Genetics, 11(10), 1185–1193. 10.1093/hmg/11.10.1185 [PubMed: 12015278]

Gould D, Smith R, & John S (2004). Anterior segment development relevant to glaucoma. International Journal of Developmental Biology, 48(8–9), 1015–1029. 10.1387/ijdb.041865dg

Gunn DJ, Gole GA, & Barnett NL (2011). Specific amacrine cell changes in an induced mouse model of glaucoma. Clinical & Experimental Ophthalmology, 39(6), 555–563. 10.1111/j.1442-9071.2010.02488.x [PubMed: 21176046]

Harazny J, Scholz M, Buder T, Lausen B, & Kremers J (2009). Electrophysiological deficits in the retina of the DBA/2J mouse. Documenta Ophthalmologica, 119(3), 181–197. 10.1007/s10633-009-9194-5 [PubMed: 19760280]

Hicks EA, Zaveri M, Deschamps PA, Noseworthy MD, Ball A, Williams T, & West-Mays JA (2018). Conditional deletion of AP-2alpha and AP-2beta in the developing murine retina leads to altered amacrine cell mosaics and disrupted visual function. Investigative Ophthalmology & Visual Science, 59(6), 2229–2239. 10.1167/iovs.17-23283 [PubMed: 29715367]

Johnson M, McLaren JW, & Overby DR (2017). Unconventional aqueous humor outflow: A review. Experimental Eye Research, 158, 94–111. 10.1016/j.exer.2016.01.017 [PubMed: 26850315]

Johnson TV, & Tomarev SI (2010). Rodent models of glaucoma. Brain Research Bulletin, 81(2–3), 349–358. 10.1016/j.brainresbull.2009.04.004 [PubMed: 19379796]

Kerr C, Zaveri M, Robinson M, Williams T, & West-Mays J (2014). AP-2α is required after lens vesicle formation to maintain lens integrity. Developmental Dynamics, 243(10), 1298–1309. [PubMed: 24753151]

Kizhatil K, Ryan M, Marchant JK, Henrich S, & John SWM (2014). Schlemm's canal is a unique vessel with a combination of blood vascular and lymphatic phenotypes that forms by a novel developmental process. PLOS Biology, 12(7), e1001912. 10.1371/journal.pbio.1001912 [PubMed: 25051267]

Lee JY, Kim YY, & Jung HR (2006). Distribution and characteristics of peripheral anterior synechiae in primary angle-closure glaucoma. Korean Journal of Ophthalmology, 20(2), 104–108. 10.3341/kjo.2006.20.2.104 [PubMed: 16892646]

Liu P, & Johnson R (2010). Lmx1b is required for murine trabecular meshwork formation and for maintenance of corneal transparency. Developmental Dynamics, 239(8), 2161–2171. 10.1002/dvdy.22347 [PubMed: 20568247]

Luo G, D'Souza R, Hogue D, & Karsenty G (1995). The matrix Gla protein gene is a marker of the chondrogenesis cell lineage during mouse development. Journal of Bone and Mineral Research, 10(2), 325–334. 10.1002/jbmr.5650100221 [PubMed: 7754814]

Mao M, Hedberg-Buenz A, Koehn D, John SW, & Anderson MG (2011). Anterior segment dysgenesis and early-onset glaucoma in nee mice with mutation of Sh3pxd2b. Investigative Ophthalmology & Visual Science, 52(5), 2679–2688. 10.1167/iovs.10-5993 [PubMed: 21282566]

Martino VB, Sabljic T, Deschamps P, Green RM, Akula M, Peacock E, Ball A, Williams T, & West-Mays JA (2016). Conditional deletion of AP-2β in the cranial neural crest results in anterior segment dysgenesis and early-onset glaucoma. Disease Models & Mechanisms, 9(8), 849–861. 10.1242/dmm.025262 [PubMed: 27483349]

Miura G, Wang MH, Ivers KM, & Frishman LJ (2009). Retinal pathway origins of the pattern ERG of the mouse. Experimental Eye Research, 89(1), 49–62. 10.1016/j.exer.2009.02.009 [PubMed: 19250935]

Moser M, Pscherer A, Roth C, Becker J, Mucher G, Zerres K, Dixkens C, Weis J, Guay-Woodford L, Buettner R, & Fassler R (1997). Enhanced apoptotic cell death of renal epithelial cells in mice lacking transcription factor AP-2beta. Genes & Development, 11(15), 1938–1948. 10.1101/gad.11.15.1938 [PubMed: 9271117]

Parrish RK, Palmberg P, Sheu WP, & XLT Study Group. (2003). A comparison of latanoprost, bimatoprost, and travoprost in patients with elevated intraocular pressure: A 12-week, randomized, masked-evaluator multicenter study. American Journal of Ophthalmology, 135(5), 688–703. 10.1016/s0002-9394(03)00098-9 [PubMed: 12719078]

Pontoriero G, Deschamps P, Ashery-Padan R, Wong R, Yang Y, Zavadil J, Cvekl A, Sullivan S, Williams T, & West-Mays J (2008). Cell autonomous roles for AP-2alpha in lens vesicle separation and maintenance of the lens epithelial cell phenotype. Developmental Dynamics, 237(3), 602–617. [PubMed: 18224708]

Quigley HA, & Broman AT (2006). The number of people with glaucoma worldwide in 2010 and 2020. British Journal of Ophthalmology, 90(3), 262–267. 10.1136/bjo.2005.081224

Reneker LW, Silversides DW, Xu L, & Overbeek PA (2000). Formation of corneal endothelium is essential for anterior segment development—A transgenic mouse model of anterior segment dysgenesis. Development, 127(3), 533–542. 10.1242/dev.127.3.533 [PubMed: 10631174]

Robertson JV, Siwakoti A, & West-Mays JA (2013). Altered expression of transforming growth factor beta 1 and matrix metalloproteinase-9 results in elevated intraocular pressure in mice. Molecular Vision, 19, 684–695. [PubMed: 23559862]

Romero P, Sanhueza F, Lopez P, Reyes L, & Herrera L (2011). c.194 A>C (Q65P) mutation in the LMX1B gene in patients with nail-patella syndrome associated with glaucoma. Molecular Vision, 17, 1929–1939. [PubMed: 21850167]

Satoda M, Zhao F, Diaz GA, Burn J, Goodship J, Davidson HR, Pierpont MEM, & Gelb BD (2000). Mutations in TFAP2B cause Char syndrome, a familial form of patent ductus arteriosus. Nature Genetics, 25(1), 42–46. 10.1038/75578 [PubMed: 10802654]

Smith BJ, Wang X, Chauhan BC, Cote PD, & Tremblay F (2014). Contribution of retinal ganglion cells to the mouse electroretinogram. Documenta Ophthalmologica, 128(3), 155–168. 10.1007/s10633-014-9433-2 [PubMed: 24659322]

Smith R, Zabaleta A, Kume T, Savinova O, Kidson S, Martin J, & John S (2000). Haploinsufficiency of the transcription factors FOXC1 and FOXC2 results in aberrant ocular development. Human Molecular Genetics, 9(7), 1021–1032. 10.1093/hmg/9.7.1021 [PubMed: 10767326]

Smith R, Zabaleta A, Savinova O, & John S (2001). The mouse anterior chamber angle and trabecular meshwork develop without cell death. BMC Developmental Biology, 1, 3. [PubMed: 11228591]

Taiyab A, Saraco A, Akula M, Deschamps P, Ball AK, Williams T, & West-Mays JA (2021). Progressive loss of retinal ganglion cells in activating protein-2beta neural crest cell knockout mice. Current Eye Research, 46(10), 1509–1515. 10.1080/02713683.2021.1901939 [PubMed: 33689532]

Tham YC, Li X, Wong TY, Quigley HA, Aung T, & Cheng CY (2014). Global prevalence of glaucoma and projections of glaucoma burden through 2040: A systematic review and meta-analysis. Ophthalmology, 121(11), 2081–2090. 10.1016/j.ophtha.2014.05.013 [PubMed: 24974815]

Toris CB, Yablonski ME, Wang YL, & Camras CB (1999). Aqueous humor dynamics in the aging human eye. American Journal of Ophthalmology, 127(4), 407–412. 10.1016/s0002-9394(98)00436-x [PubMed: 10218693]

Tümer Z, & Bach-Holm D (2009). Axenfeld-Rieger syndrome and spectrum of PITX2 and FOXC1 mutations. European Journal of Human Genetics, 17(12), 1527–1539. 10.1038/ejhg.2009.93 [PubMed: 19513095]

Waring GO 3rd, Bourne WM, Edelhauser HF, & Kenyon KR (1982). The corneal endothelium. Normal and pathologic structure and function. Ophthalmology, 89(6), 531–590. 10.1016/S0161-6420(82)34746-6 [PubMed: 7122038]

Weinreb RN, Aung T, & Medeiros FA (2014). The pathophysiology and treatment of glaucoma: A review. JAMA, 311(18), 1901–1911. 10.1001/jama.2014.3192 [PubMed: 24825645]

West-Mays JA, Zhang J, Nottoli T, Hagopian-Donaldson S, Libby D, Strissel KJ, & Williams T (1999). AP-2alpha transcription factor is required for early morphogenesis of the lens vesicle. Developmental Biology, 206(1), 46–62. [PubMed: 9918694]

Winkler NS, & Fautsch MP (2014). Effects of prostaglandin analogues on aqueous humor outflow pathways. Journal of Ocular Pharmacology and Therapeutics, 30(2–3), 102–109. 10.1089/jop.2013.0179 [PubMed: 24359106]

Wright C, Tawfik MA, Waisbourd M, & Katz LJ (2016). Primary angle-closure glaucoma: An update. Acta Ophthalmologica, 94(3), 217–225. 10.1111/aos.12784 [PubMed: 26119516]

## Significance

Abnormalities in anterior ocular structures including the trabecular meshwork (TM) and Schlemm's canal (SC) can increase intraocular pressure (IOP), which can damage retinal ganglion cells (RGCs). The current study showed that deletion of transcription factor activating protein 2-beta (AP-2β) using the Mgp-Cre knock-in (Mgp-Cre.KI) from the developing TM region leads to abnormal TM and SC development, causing elevated IOP. Increased IOP reduced upon treatment with latanoprost, which increases outflow through the unconventional pathway. Moreover, elevated IOP was correlated with progressive RGC loss and reduced retinal function. The AP-2β mutant can model human glaucoma to test IOP-lowering drugs and neuroprotective strategies.

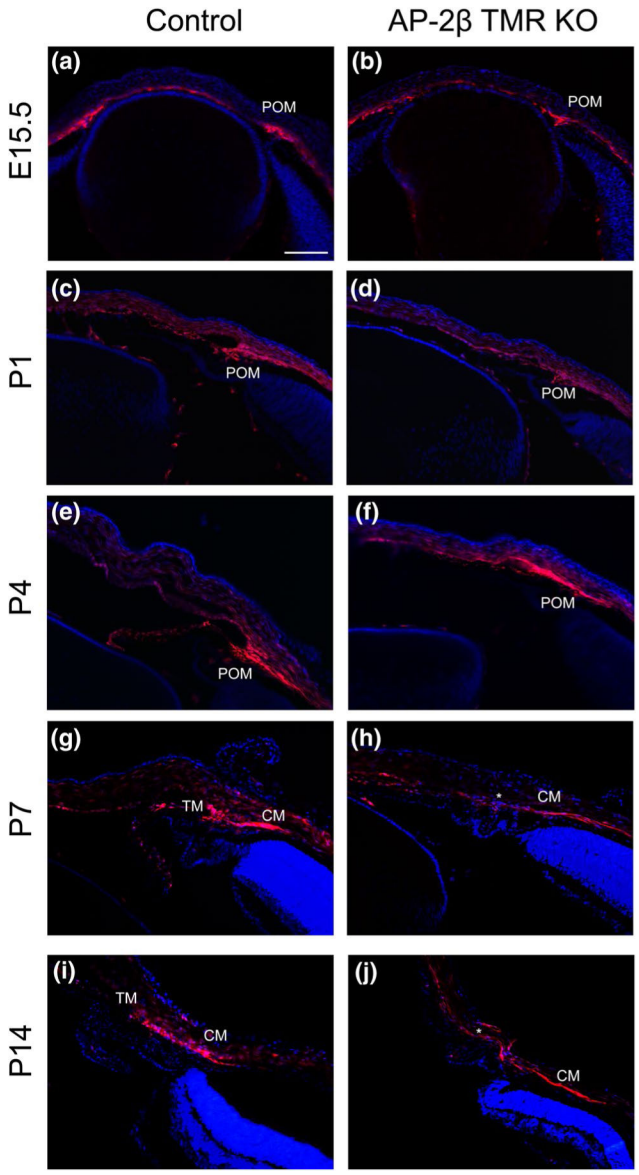


**FIGURE 1.**

Fate mapping of *Mgp*-Cre.KI using tdTomato in embryonic and postnatal controls versus AP-2β TMR KOs. (a,b) At E15.5 (*n* = 3 eyes), tdTomato—which marks cells expressing *Mgp*-Cre.KI, or the descendants of such cells—is expressed in the developing POM. No observable difference in NCC migration is present between the TMR KO and controls. (c,d) At P1 (*n* = 3 eyes), there is also no difference in tdTomato expression in the iridocorneal angle of the TMR KO mice compared with controls. (e,f) At P4 (*n* = 3 eyes), there appears to be a mild decrease in tdTomato expression in the iridocorneal angle region. (g–j) At both P7 (*n* = 3 eyes) and P14 (*n* = 3 eyes), there also appears to be a reduction in expression of tdTomato in the iridocorneal angle of the TMR KO mice compared with controls. Asterisks in panels h,j show the prospective iridocorneal angle region. CM, ciliary muscle; POM, periocular mesenchyme; TM, trabecular meshwork. Scale bar represents 100 μm. Images were acquired using a 20× objective lens

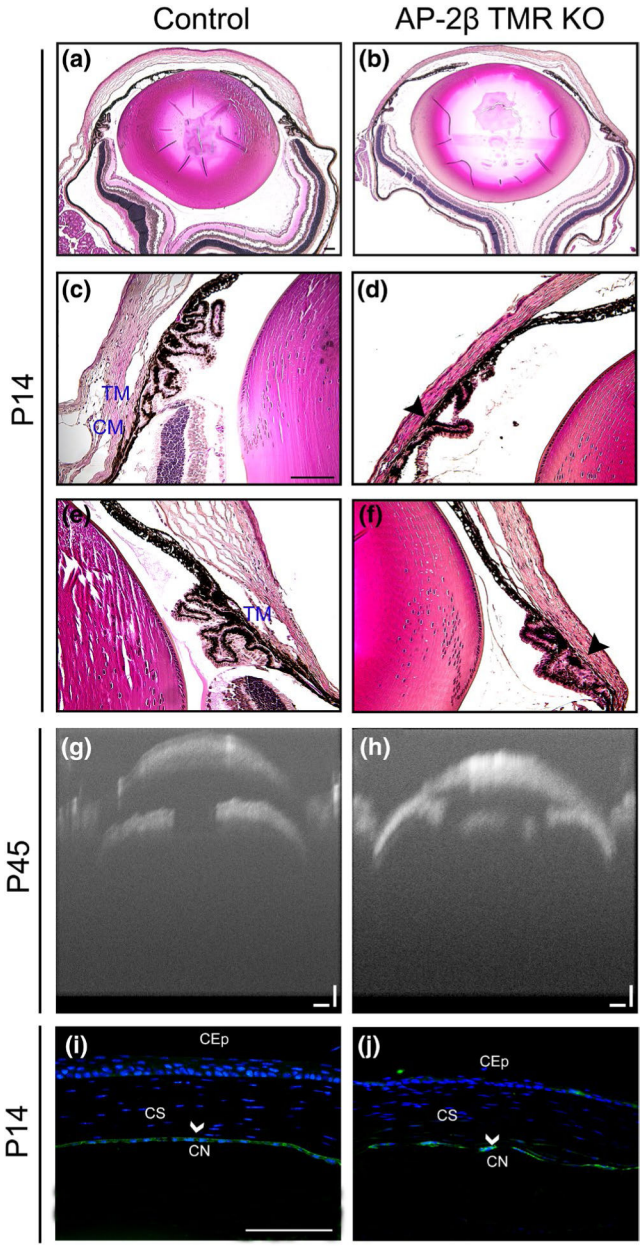


**FIGURE 2.**

Abnormal morphology of the TM in AP-2β TMR KO mice as compared with control mice. (a,b) By P14, the TM region appears to be absent in the TMR KO when compared with control mice ($n$ = 6 eyes). (c–f) Higher magnification images of (a) and (b) are depicted in (c,e) and (d,f), respectively. (g,h) OCT images show a fully open iridocorneal angle in P45 control mice (g; $n$ = 6 eyes). The AP-2β TMR KO angle is partially closed (h), displaying PAS. Scale bar, 250 μm. (i,j) At P14 ($n$ = 3 eyes), N-cadherin expression is present in both control and AP-2β TMR KO mice. CEp, corneal epithelium; CM, ciliary muscle; CN, corneal endothelium; CS, corneal stroma; TM, trabecular meshwork. Scale bars in panels a–f and panels i,j represent 100 μm. Images a,b were acquired using a 5× objective lens,

images c–f were acquired using a 20× lens, and images i,j were acquired using a 40× objective lens

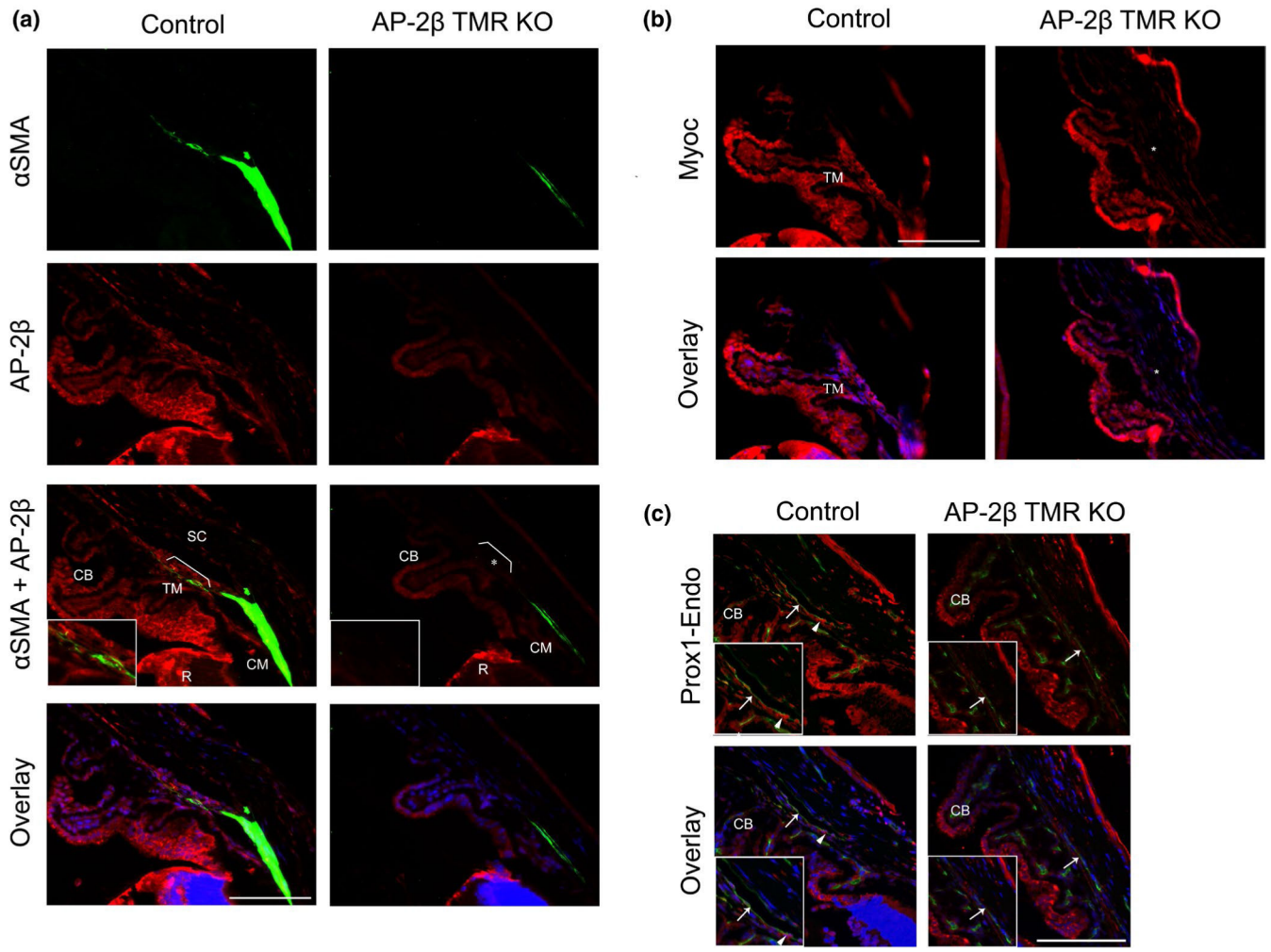


**FIGURE 3.**

Loss of AP-2β in TMR KOs causes reduced expression of TM and SC markers. (a) In P14 control mice, AP-2β is detected in the iridocorneal angle, as well as the retina (R) and ciliary body (CB). In P14 AP-2β TMR KO animals ($n$ = 6 eyes), AP-2β is still observed in the ciliary body and retina but is now absent from the iridocorneal angle (TMR KO panel showing αSMA and AP-2β co-staining, bracketed region also shown as inset). αSMA expression is also reduced in the TM region of TMR KO mice compared with control mice. (b) At P14 ($n$ = 6 eyes) in controls, there is extensive myocilin expression within the angle tissue, the corneal epithelium, and the ciliary body, but expression is specifically lost in the angle tissue of TMR KO mice (AP-2β TMR KO panels, asterisks). (c) Co-staining of Prox1 (red) and endomucin (green) shows a defined and open SC region in the control angle (control panels; endomucin staining marked by the arrow), whereas the TMR KO angle shows a hypoplastic SC (AP-2β TMR KO panels; endomucin staining marked by the arrow). Furthermore, there appears to be a reduction in Prox1 staining in this region in the TMR KO when compared with the control SC (control panels, insets, Prox1 staining marked by the arrowhead). CB, ciliary body; CM, ciliary muscle; R, retina; SC, Schlemm's canal;

TM, trabecular meshwork. Scale bars represent 100 μm. Images were acquired using a 40× objective lens

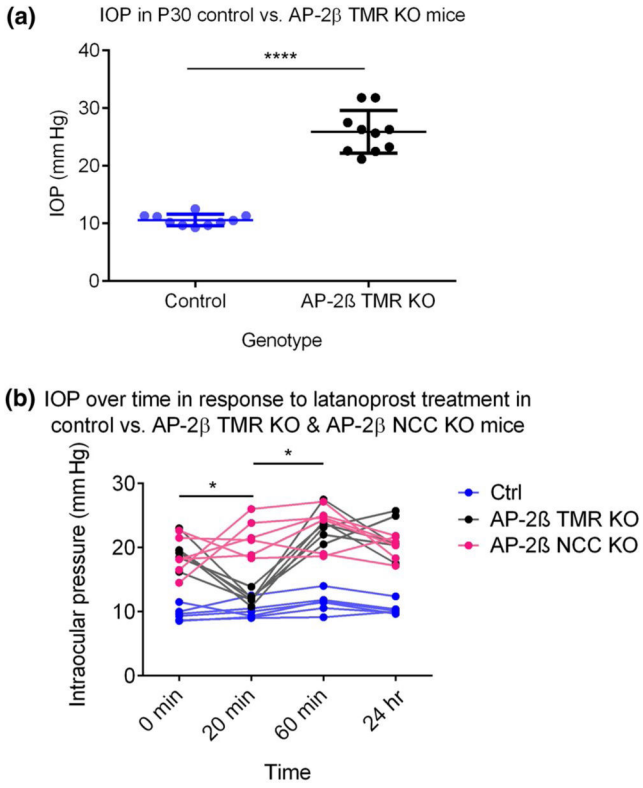


**FIGURE 4.**

Increased IOP resulting from partial angle closure in AP-2β TMR KOs reduces upon latanoprost treatment. (a) There is a significant increase in IOP in the AP-2β TMR KO mice at P30 ($n = 10$ eyes; $t_{18} = 12.57$; $p < 0.0001$; two-sided independent $t$ test; all error bars signify standard deviation) when compared with control mice. (b) IOP in the AP-2β TMR KO is significantly lower at 20 min after latanoprost treatment ($n = 6$ eyes; two-way repeated measures ANOVA, Tukey's post hoc test; $F_{(2,40)} = 169.8$; $p < 0.0001$) when compared to its own baseline IOP. By 60 min of post-treatment, TMR KO IOP increases significantly compared to the IOP at 20 min ($p < 0.0001$). On the other hand, AP-2β NCC KO mice display high IOP both before and after latanoprost treatment ($n = 6$ eyes; $p < 0.0001$ for all time points analyzed compared with controls)

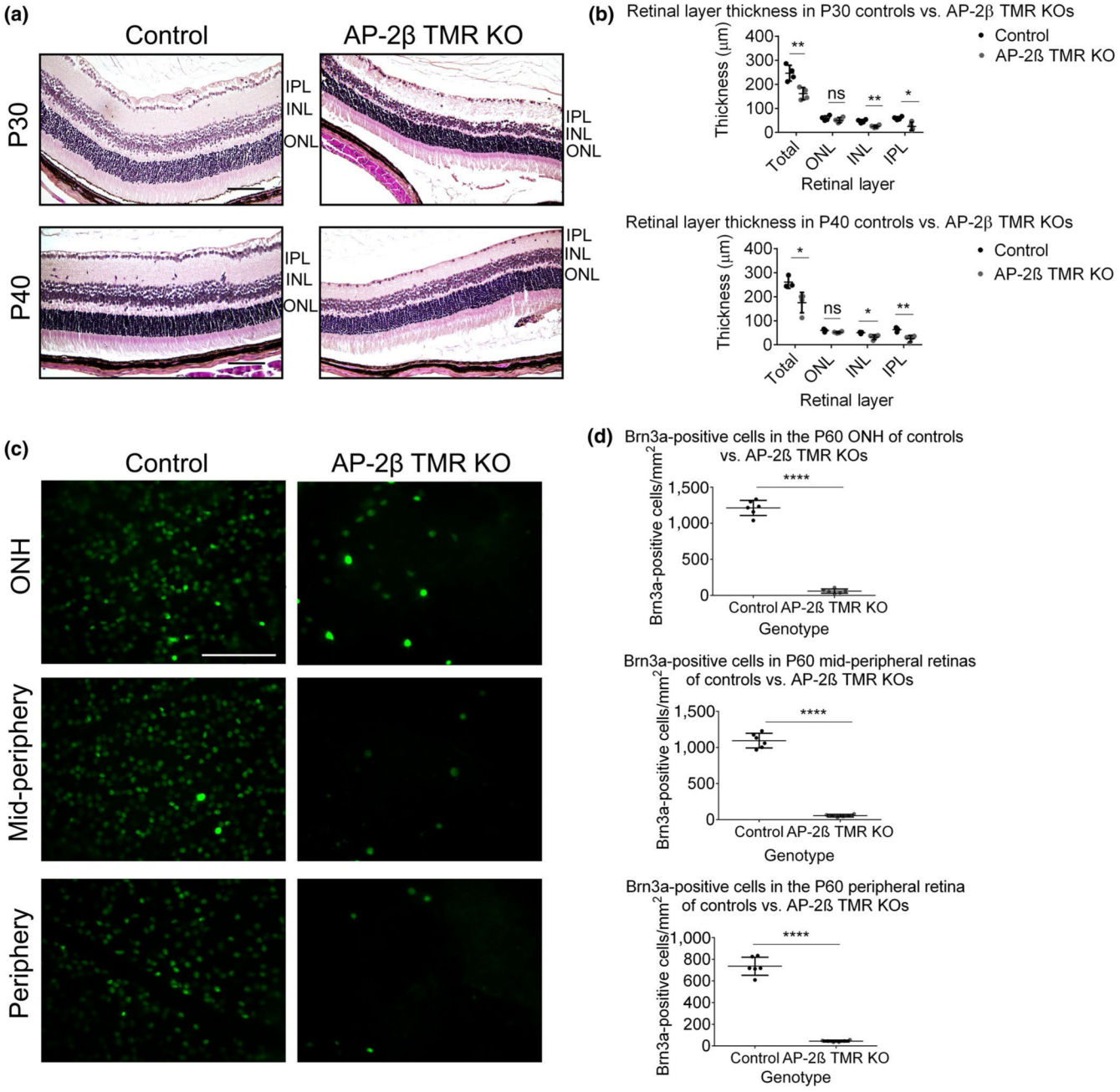


**FIGURE 5.**

Reduced retinal, INL, and IPL thickness, and reduced Brn3a cell count in AP-2β TMR KOs. (a,b) At P30 (a minimum of $n = 3$ eyes), there is a significant reduction in total retinal thickness (two-sided independent $t$ test; $t_6 = 4.12$; $p < 0.01$; all error bars represent standard deviation), as well as thickness of the INL ($t_6 = 4.83$; $p < 0.01$) and IPL ($t_6 = 3.68$; $p < 0.05$) in the TMR KOs when compared with controls. At P40 (a minimum of $n = 3$ eyes; two-sided independent $t$ test), there continues to be a significant reduction in total retinal thickness ($t_5 = 3.05$; $p < 0.05$), as well as thickness of the INL ($t_5 = 3.04$; $p < 0.05$) and IPL ($t_5 = 4.11$; $p < 0.01$) in the TMR KOs when compared with controls. (c,d) There is a significant reduction in the number of Brn3a-positive cells in flat mounted retinas of TMR KOs when compared

with control retinas in the region adjacent to the ONH, mid-periphery and peripheral regions of the retina ($n = 6$ eyes; two-sided independent $t$ test for each region; $t_{10} = 25.87$ for the ONH, $t_{10} = 24.69$ for the mid-peripheral region, $t_{10} = 20.19$ for the peripheral region; $p < 0.0001$ for all three regions). INL, inner nuclear layer; IPL, inner plexiform layer; ONL, outer nuclear layer. Scale bars represent 100 μm. Images in (a) were acquired using a 20× objective lens, and images in (c) were acquired using a 40× objective lens

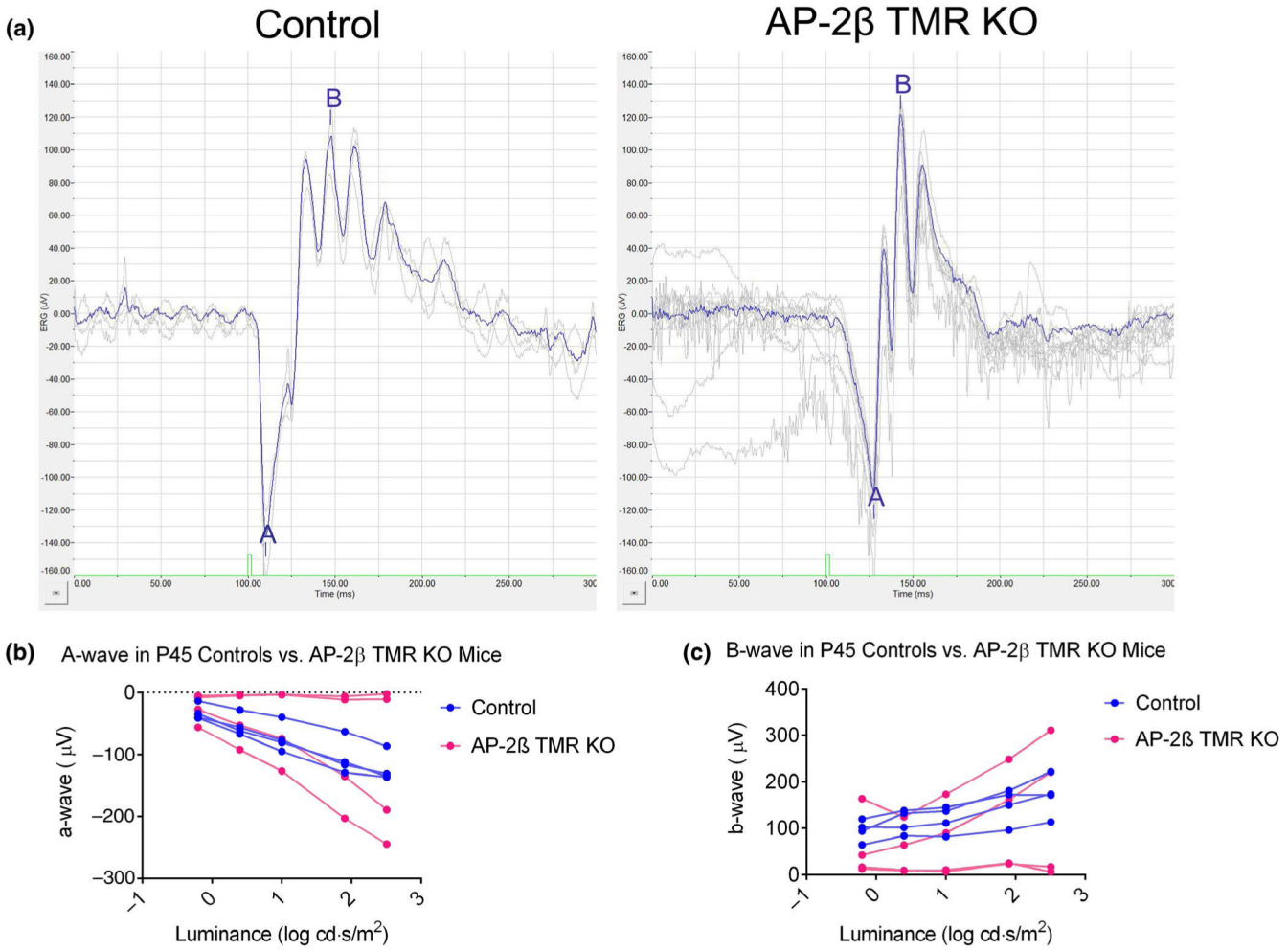


**FIGURE 6.**

The a-wave and b-wave measured using ERGs in P45 controls and AP-2β TMR KOs. (a) Sample ERG traces of the a-wave and b-wave of P45 controls and TMR KOs show that the b-wave peak is similar in appearance in both the control and TMR KO (peaks labeled “B”). (b) There is no significant difference in the amplitude of the a-wave in TMR KO mice when compared to control mice in response to 2-ms flashes of light (504 nm) between −0.2 and 2.5 cd·s/m$^2$ (log scale) in intensity (a minimum of $n = 3$ eyes; two-way repeated measures ANOVA; $F_{(1,6)} = 0.15$; all error bars represent standard deviation). (c) There is no significant difference in the amplitude of the b-wave in TMR KO mice when compared to control mice in response to 2-ms flashes of light between −0.2 and 2.5 cd·s/m$^2$ (log scale) in intensity (a minimum of $n = 3$ eyes; two-way repeated measures ANOVA; $F_{(1,6)} = 0.79$)

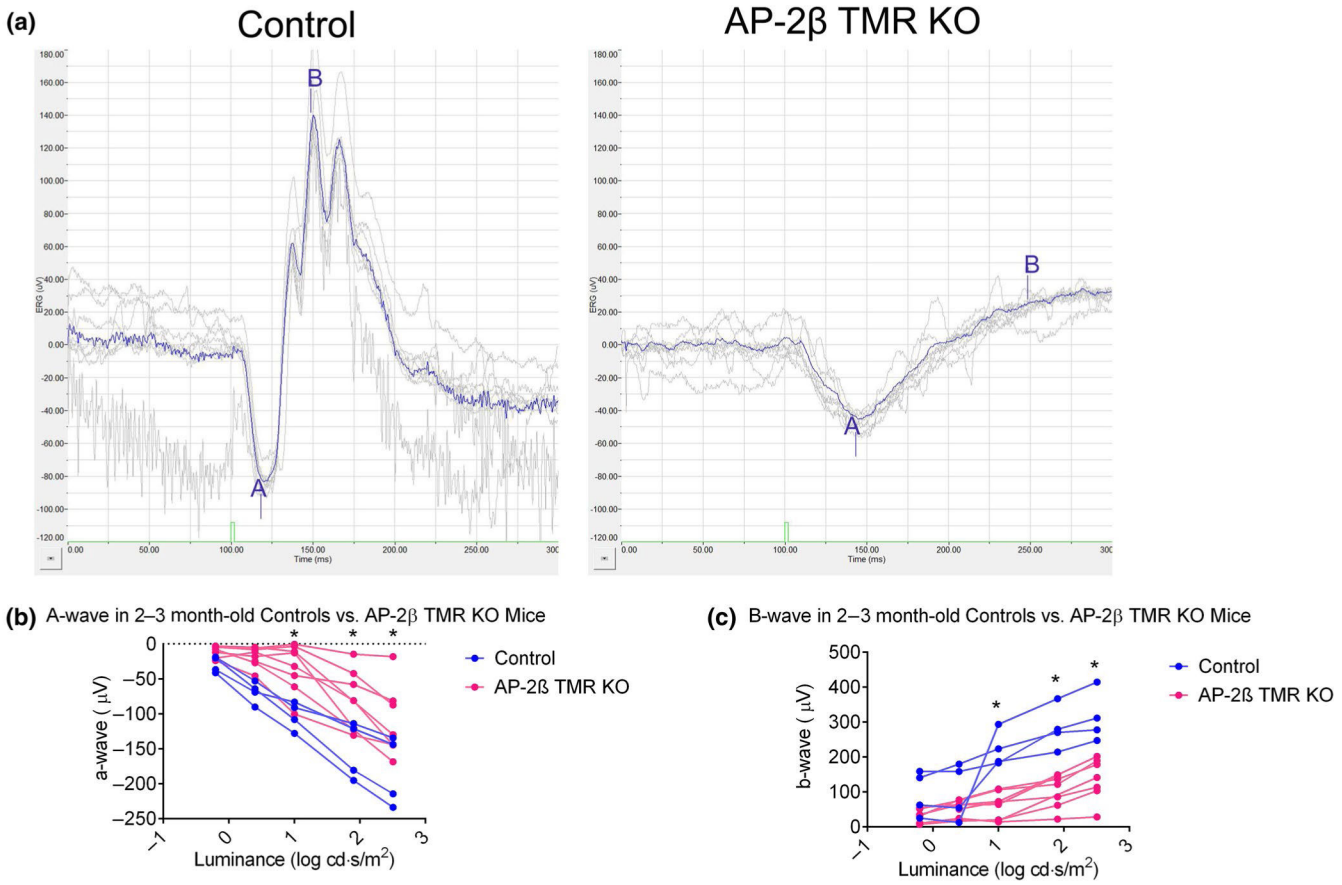


**FIGURE 7.**

The a-wave and b-wave measured using ERGs in 2- to 3-month-old controls and AP-2β TMR KOs. (a) Sample ERG traces of the a-wave and b-wave of 2- to 3-month-old controls and TMR KOs show that the b-wave peak is not visible in the TMR KO trace (AP-2β TMR KO panel; region labeled “B”), whereas the control trace shows a b-wave peak (control panel; peak labeled “B”). (b) There is a significant reduction in the amplitude of the a-wave in TMR KO mice when compared to control mice in response to 2-ms flashes of light (504 nm) between 1 and 2.5 cd·s/m$^2$ (log scale) in intensity (a minimum of $n = 3$ mice; mixed model, Bonferroni post hoc method; $F_{(1,10)} = 12.81$; $p < 0.05$ for the last three flash intensity values; all error bars represent standard deviation). (c) There is a significant reduction in the amplitude of the b-wave in TMR KO mice when compared to control mice in response to 2-ms flashes of light between 1 and 2.5 cd·s/m$^2$ (log scale) in intensity (a minimum of $n = 3$ mice; mixed model, Bonferroni post hoc method; $F_{(1,10)} = 37.00$; $p < 0.05$ for the last three flash intensity values)

**TABLE 1**

Antibody details.

| Name | Structure of immunogen | Manufacturer, RRID & species | Concentration |
|---|---|---|---|
| AP- 2β | A synthetic peptide to the AP-2β sequence | Cell Signalling 2509S – AB_2058198 – Rabbit polyclonal | 1:50 |
| αSMA | Single isoform α-actin | Sigma Aldrich A2547 – AB_476701 – Mouse monoclonal | 1:100 |
| Myocilin | Synthetic peptide corresponding to N-terminal amino acids 25– 46 of Myocilin | FabGennix MYO-101AP – Rabbit polyclonal | 1:200 |
| Prox1 | C-terminal 15 amino acids of mouse Prox1 | Covance – 925201 – Rabbit polyclonal | 1:100 |
| Endomucin | Mouse endomucin protein | eBioscience 14– 5851-82 – AB_2749865 – Rat monoclonal | 1:100 |
| N-Cadherin | Mouse N-Cadherin amino acids 802– 819 | BD Transduction 610920 – AB_2077527 – Mouse monoclonal | 1:100 |
| Brn3a | Epitope mapping near the N terminus of Brn3a of human origin | Santa Cruz sc-8429 – AB_626765 –Rabbit polyclonal | 1:100 |
| Secondary antibodies | IgG (H+L) | Alexa Fluor – Donkey polyclonal raised against goat (AB_2534102) or goat polyclonal raised against rabbit (AB_143157), mouse (AB_2536161), or rat (AB_2534074) | 1:200 |